High-Performance Ambipolar Transistors and Inverters from an Ultralow Bandgap Polymer

*Jian Fan, Jonathan D. Yuen, Mingfeng Wang, Jason Seifter, Jung-Hwa Seo, Ali Reza Mohebbi, Dante Zakhidov, Alan Heeger, and Fred Wudl**

Ambipolar organic thin-film transistors (OTFTs) with high hole and electron mobilities have attracted considerable attention due to their application in complementary metal-oxide semiconductor (CMOS) digital integrated circuits.[1] Due to their processing simplicity, solution processable single component ambipolar polymers have great advantage over blend and bilayer systems of unipolar semiconductors in the construction of ambipolar OTFTs. In ambipolar blend systems, the ambipolar charge transport and the associated carrier mobilities in blend system have a complex dependence on the blend composition and the phase-separated morphology, and therefore are highly dependent on processing conditions.[1c] In ambipolar bilayer systems, the bilayer is often fabricated via vacuum deposition of small molecule as solution processed bilayer films are difficult to realize since they require the second layer to be processable with solvents orthogonal to that of the initial layer.[1e–f] Research in the design and syntheses of ambipolar polymers has witnessed remarkable progress in recent years and both hole and electron mobilities of these materials have reached and even exceeded 0.1 $cm^2V^{-1}s^{-1}$,[2] ambipolar polymers with higher performance are still desirable for high-end applications. Since the low-lying lowest unoccupied molecular orbital (LUMO) and high-lying highest occupied molecular orbital (HOMO) levels would facilitate the efficient injection and transport of electrons and holes, the coupling of strong donor with strong acceptor monomers could be a promising synthetic strategy to realize effective ambipolar field effect transistors.

Most conjugated polymers exhibit p-type mobility. It is interesting to note that polymer poly(diketopyrrolopyrrolebithiophene-thienothiophene) (PDBT-co-TT) predominantly shows p-type mobility,[3] but when thieno[3,2-b]thiophene, the donor part in PDBT-co-TT, is replaced with a benzothiadiazole accepting unit, the resulting polymer poly(diketopyrrolopyrrole-thiophenebenzothiadiazolethiophene) (PDPP-TBT) becomes a typical ambipolar semiconductor.[2c] While the selection of a proper acceptor can be the key step to achieve high performance ambipolar transport, so far only a few acceptors have been successfully developed for this purpose. During the last decade, strong acceptors such as diketopyrrolopyrrole (DPP),[2,4] and naphthalene bisimide[5] have been extensively investigated due to their special optical and electrochemical properties and outstanding stabilities. It was only recently that benzobisthiadiazole (BBT) unit has been incorporated into donor-acceptor (DA) polymers.[6] The BBT unit shows very high electron affinity, which is ascribed to its 14π electron system containing a tetravalent sulfur atom. It will generate a more stable Kekulé-type thiadiazole moiety upon accepting an electron. The inter-chain interaction can be reinforced by S···N intermolecular contact effects between BBT units.[7] We have previously synthesized a family of DA polymers with BBT as the acceptor moiety, observing that ambipolar behavior is universal for these polymers.[8]

Herein we report a new BBT based polymer poly (benzobisthiadiazole bithiophene-thienothiophene) **PBBTTT** with a bi(thiophen-2-yl)-thieno[3,2-b]thiophene unit located between each pair of BBT units along the chain. This semiconducting polymer exhibits nearly balanced hole and electron mobilities as high as 1.0 and 0.7 $cm^2V^{-1}s^{-1}$, respectively. Using the ambipolar polymer, inverters have been demonstrated with a gain of 35; i.e. much higher than values usually obtained for unipolar logic.

The thiophene-BBT-thiophene monomer exhibits relatively low solubility even after being modified with straight alkyl chains (hexyl or dedecyl group). Inspired by the introduction of long branched solublizing groups in DPP[2] and rylene bisimides systems,[9] we decorate the thiophene-BBT-thiophene monomer with two 2-octyl-1-dodecyl groups (**Scheme 1**), thus increasing the solubility of the resultant polymer. Tail-to-tail regiopositioning of the alkyl chains would minimize any steric interactions between BBT unit and the alkyl groups, thus preserving backbone planarity. Polymer **PBBTTT** was synthesized via the Stille copolymerization between 4,7-bis-[5-bromo-4-(2-octyldodecyl)-thiophen-2-yl]-benzobisthiadiazole (**1**) and 2,5-bis-trimethylstannanyl-thieno[3,2-b]thiophene (**2**). This coupling reaction uses two symmetrical monomers, thus avoiding the regioirregularity that can occur during the polymerization of asymmetric monomers. **PBBTTT** was purified by soxhlet extraction using methanol, hexane and dichloromethane (DCM) successively to remove the impurities and oligomers.

Dr. J. Fan,[+] Prof. A. Heeger, Prof. F. Wudl
Center for Energy Efficient Materials
University of California
Santa Barbara, CA 93106, USA
E-mail: wudl@chem.ucsb.edu
Dr. J. Fan, Dr. J. D. Yuen,[+] Dr. M. Wang,
J. Seifter, Dr. J. Seo, Dr. A. R. Mohebbi, D. Zakhidov,
Prof. A. Heeger, Prof. F. Wudl
Center for Polymers and Organic Solids
University of California
Santa Barbara, CA 93106, USA
Dr. J. Seo
Department of Materials Physics
Dong-A University
Busan 604-714, Republic of Korea
[+] Equal contribution from J. Fan and J. D. Yuen.

DOI: 10.1002/adma.201103836

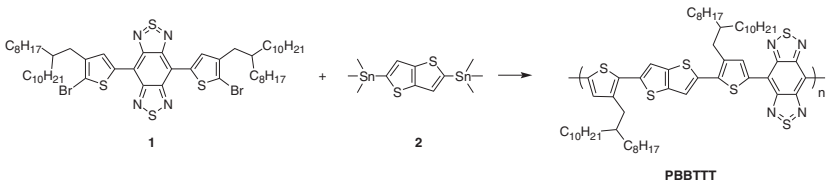

Scheme 1. Synthesis of PBBTTT *via* Stille coupling polymerization

The remaining crude product in the thimble was then extracted with chloroform, and precipitated out by the addition of methanol. The number average molecular weight (Mn) was 15.1 kDa, with a polydispersity index (PDI) of 1.94. The PDI was determined by using gel permeation chromatography (GPC) at 150 °C in 1,2,4-trichlorobenzene against polystyrene standards. The optical properties of **PBBTTT** in chloroform and as a thin film were studied using UV-vis-NIR spectroscopy. The absorption onset of around 2200 nm in the solid state corresponds to an optical bandgap of 0.56 eV, as shown in Figure S1 in the Supporting Information (SI). The electrochemical properties of **PBBTTT** were investigated by cyclic voltammetry (CV) in order to determine the HOMO and/or LUMO energy levels (Figure S2 in the SI). The LUMO value of **PBBTTT** was calculated from the onset reduction potential, which was –3.80 eV, whereas the HOMO value of –4.36 eV was determined from the difference between the LUMO and the optical bandgap. Differential scanning calorimetry (DSC) shows no thermal transition between 40–300 °C, as shown in Figure S3 in the SI.

In order to investigate the crystallinity and microstructure of the polymer thin film, X-ray diffraction (XRD) and Atomic Force Microscopy (AFM) measurements were carried out. As shown in **Figure 1**, the specular out-of-plane X-ray diffraction pattern for an as-cast film was essentially featureless. Significant annealing-induced sharpening of the diffraction peaks at around 4° was observed. Both observations indicated that the microstructure of the as-cast film was kinetically limited and the polymer chains

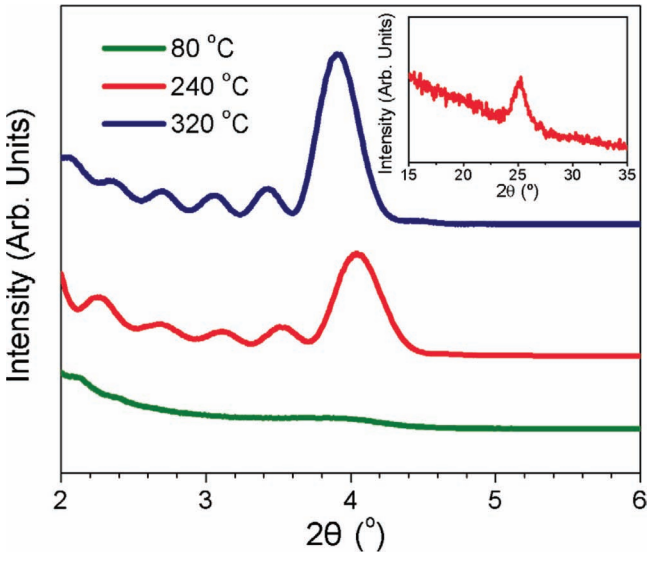

Figure 1. XRD data obtained from spin-coated PBBTTT thin films on decyltrichlorosilane-modified SiO_2/Si substrates annealed at different temperatures. The inset shows the in-plane profile at 240°.

reorganized to ordered lamellar crystalline structures upon annealing. The annealed samples showed enlarged out-of-plane d-spacing from 21.84 Å ($2\theta = 4.04°$) at 240 °C to 22.57 Å ($2\theta = 3.91°$) at 320 °C. This may be due to less backbone inclination from the substrate, relaxation of side-chain resulting in less dense side chain packing/interdigitation, or an increase of the angle which the side chains make with the backbone.[10] The additional peaks at 240 °C and 320 °C are associated with Kessig interference[11] from substrate reflection. In the in-plane grazing incidence profile, a diffraction peak was observed at $2\theta = 25.25°$ ($d = 3.53$ Å) when the film was annealed at 240 °C. This very short π–π stacking distance implies strong interactions between "edge-on" orientated polymer chains.

AFM height image of PBBTTT thin films annealed at 80 °C show randomly-oriented nanorods (**Figure 2**). Upon annealing at 240 °C, a highly interconnected fiber structure was observed. When annealed at 320 °C, the polymer thin film forms uniform polymer fibers that establish the more ordered multiple-layer structure with an obvious reduction of the surface roughness, which is in good agreement with XRD results.

Transistors of **PBBTTT** were fabricated and tested to determine the effect of the BBT moiety on the performance of the resulting device. Bottom-gate, Au bottom-contact transistors were fabricated with **PBBTTT** as the active layer on heavily-doped silicon substrates. The insulator used was a 200 nm SiO_2 layer passivated with decyltrichlorosilane (DTS). All devices were tested and annealed in nitrogen-purged gloveboxes. Samples measured had channel lengths of 5μm and channel widths of 1mm. The transfer and output characteristics of a typical **PBBTTT** transistor, annealed at 240 °C, are shown in **Figure 3** with transfer curves in the inset. $I_{DS}^{1/2}$ and I_{DS} are plot as a function of V_{GS} in Figure S4 in the Supporting Information. We observe that the slope of $I_{DS}^{1/2}$ vs. V_{GS} is linear for a large range of gate voltages, particularly at low gate voltages where saturation is observed for p-type transport, and for all gate voltages for n-type transport. High performance ambipolar behavior can be clearly observed in both the transfer and output characteristics, with currents in the hundreds of microamperes. In ambipolar OTFTs[12] the transfer curves trace a V-shaped trough with decreasing magnitude of gate voltage, indicating a transition from unipolar to ambipolar behavior. This is reflected in the output plots exhibiting, at high gate voltages, unipolar transport with standard linear-to-saturation current-voltage (IV) transistor characteristics and, at low gate voltages, ambipolar transport with diode-like IV characteristics. The air stability of **PBBTTT** was found to be similar to other BBT-based materials.[8]

The inclusion of the BBT unit in the polymer results in an ultra-low bandgap with high LUMO and HOMO energy levels which enable ease of injection for holes and electrons. The ease of injection of charges is further improved via oxidation of the Au source-drain contacts exposed UV-ozone treatment. It was found from UPS measurements (Figure S5 in the SI) that the work function of Au was reduced from 4.9 eV to 4.4 eV treatment, close to both the LUMO and HOMO of **PBBTTT**. It is worthy of note that polymer PDBT-co-TT is basically a p-type semiconductor,[3] while **PBBTTT** exhibits ambipolar behavior. This result was ascribed to the facts that BBT is a much

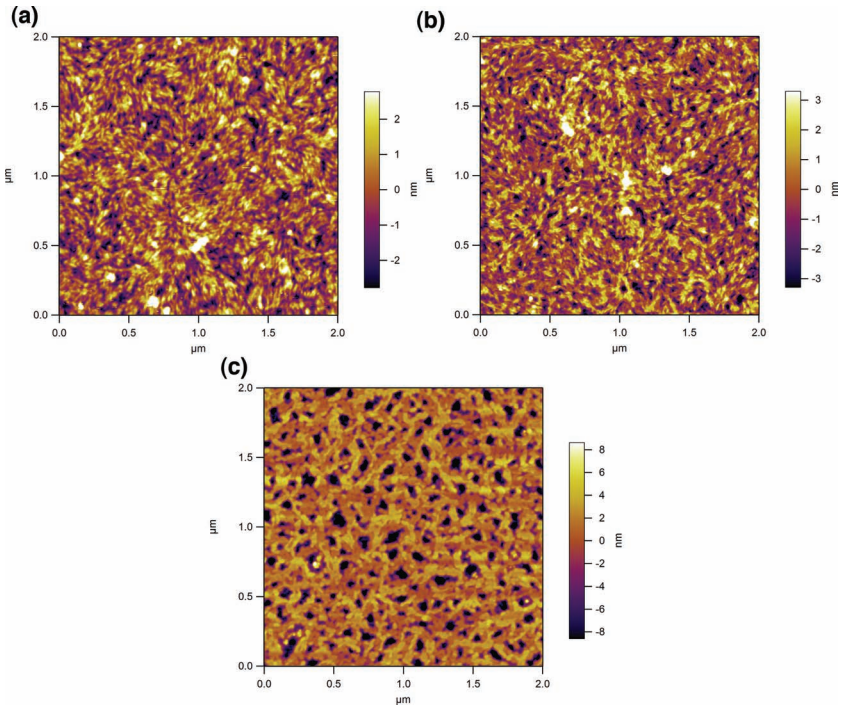

Figure 2. AFM phase images of PBBTTT thin films at 80 °C (a), 240 °C (b) and 320 °C (c) on decyltrichlorosilane-modified SiO_2/Si substrates.

stronger acceptor than DPP and LUMO of PBBTTT (–3.8 eV, as directly determined by CV) is much deeper than that of PDBT-co-TT (–3.4 eV, also directly determined by CV). Furthermore, the π–π distance between polymer backbones in PBBTTT (3.53 Å) is much smaller than that observed in PDBT-co-TT (3.71 Å), which is favorable for charge transfer via hopping.

To more accurately quantify and compare device performance, charge-carrier mobilities in the unipolar regimes were calculated with the standard equation used to describe MOS field effect transistors operating in the saturation regime: $I_{DS} = ½(W/L)\mu C_i(V_G–V_T)^2$, with mobility determined from $\partial|I_{DS}|^{1/2}/\partial V_G$. In order to determine the effect the observed structural ordering has on transport behavior, the transistor samples were annealed at different temperatures. Both n-type and p-type mobilities as a function of annealing temperature are shown on **Figure 4**, for a set of 11 transistors. The performance is high for all temperatures, with most devices showing p-type and n-type mobilities above 0.1 $cm^2V^{-1}s^{-1}$ for all annealing temperatures. Some devices exhibit mobilities as high as 1.0 $cm^2V^{-1}s^{-1}$ for p-type transport, with n-type transport reaching a maximum of 0.7 $cm^2V^{-1}s^{-1}$. The highest average mobility for p-type performance was 0.6 $cm^2V^{-1}s^{-1}$ at 240 °C and 0.3 $cm^2V^{-1}s^{-1}$ at 280 °C for n-type, with average mobilities remaining above 0.1 $cm^2V^{-1}s^{-1}$ for all annealing temperatures. An exception is at 350 °C, where the average n-type mobility drops to 0.02 $cm^2V^{-1}s^{-1}$ (indicative of degradation).

While the spread of n-type mobility was large among the devices, n-type mobility for each individual device remained nearly unchanged at different annealing temperatures. In contrast, p-type mobilities increased with annealing temperature up to 240 °C, indicating that transport improved with the increase in the alignment of the grains with the substrate. However, from 240 to 320 °C, the mobility remains constant despite the significant morphological change observed in the AFM images. For example, pinhole-like voids are observed in thin films when annealed at 320 °C, which implies poor connectivity between fibers and reduced surface coverage. So correlation between performance and morphology is not simple in this case. Increased mobility would be expected, as the increase

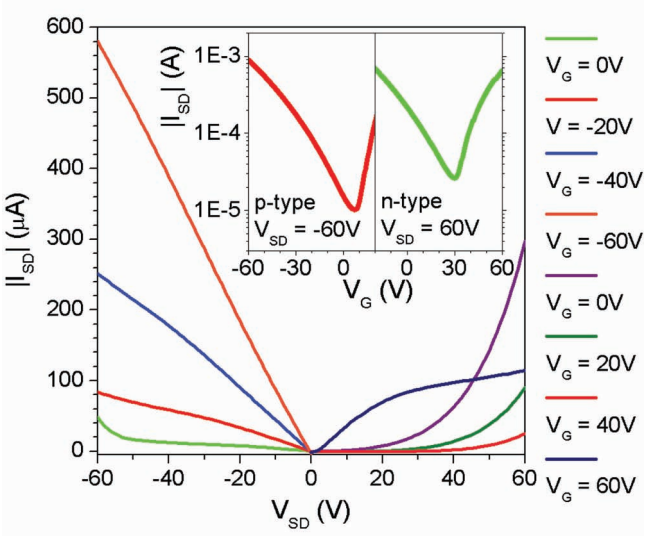

Figure 3. Transfer (inset) and output characteristics of a PBBTTT transistor annealed at 240 °C.

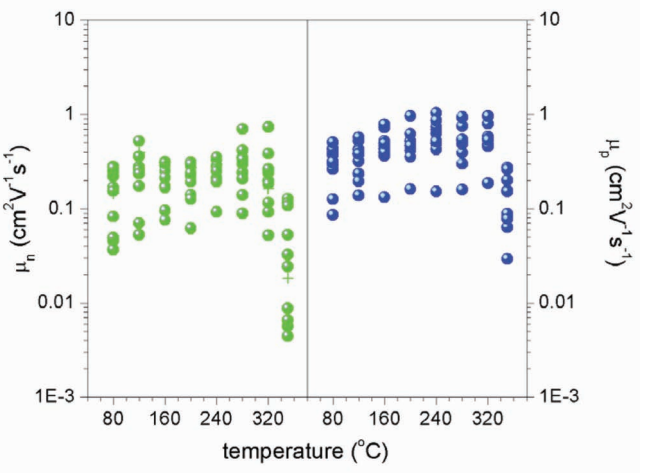

Figure 4. Transistor mobilities as a function of annealing temperature for PBBTTT.

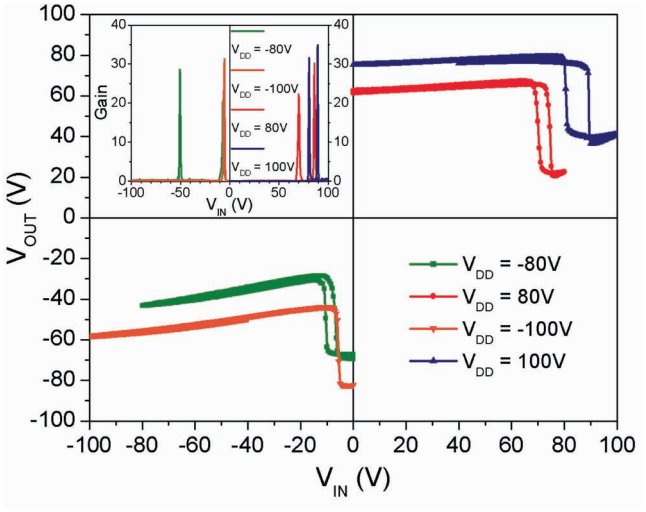

Figure 5. Inverter characteristics of an inverter based on two identical PBBTTT FETs.

of ordering can be clearly observed in both AFM and XRD measurements.

Given the ambipolar nature and high performance of PBBTTT OTFTs, two identical ambipolar transistors were combined into an inverter circuit, with the common gate as the input voltage. Inverting functionality was clearly observed both in the first and the third quadrant, with the input voltage (V_{IN}) and the supply voltage (V_{DD}) being both positively or negatively biased (**Figure 5**). It is noted that an asymmetry in the inverter transfer curve is observed, with inversion occuring at a lower magnitude of V_{IN} in the negative quadrant compared to the positive quadrant. This observation mirrors the asymmetry observed in the transistor transfer curves in Figure 3. From the steepness of inverter curve, the maximum gain of ca 35 is obtained, which is higher than 6,[13a] 15,[4b] 20,[13b] and 30[4a,5] in the CMOS-like inverters based on ambipolar FETs but not as high as 86, reported by Sirringhaus.[10]

In conclusion, we reported a new DA conjugated polymer PBBTTT based on a strong acceptor BBT unit. Long branched solubilizing groups, 2-octyl-1-dodecyl, were introduced into BBT monomer, and the resulting polymer exhibited good solubility in various solvents. XRD measurement reveals that upon thermal annealing, intimate interaction between edge-on orientated polymer chains is observed with π–π stacking distance as low as 3.53Å. The strong interaction between strong acceptor and strong donor in this polymer leads to an ultra-low bandgap with LUMO at –3.8 eV and HOMO at –4.36 eV. As a result, the hole and electron mobilities of PBBTTT are as high as 1.0 $cm^2\ V^{-1}\ s^{-1}$ and 0.7 $cm^2\ V^{-1}\ s^{-1}$, respectively. The inverter based on two identical ambipolar transistors exhibits a high gain of around 35.

Experimental Section

Fabrication and characterization of FET devices: Transistors were fabricated in the bottom gate, bottom contact configuration on heavily-doped n-type Si substrates as the gate and thermally grown 200 nm silicon dioxide as the dielectric layer (Silicon Quest, dry oxide). The source and drain electrodes were patterned using standard photo-lithography and formed on SiO_2 with e-beam evaporation of a sticking layer 3 nm of nickel and a covering layer of 47 nm of inert gold. Prior to casting, devices were cleaned in acetone and isopropanol and dried in an oven at 120 °C for 15 min. The samples were then surface-activated with acid hydrolysis, dried and then exposed for 30 min to UV light in air. The devices were surface treated with DTS for 30 min by immersion in a 1% by volume of DTS in toluene. The devices were then cleaned by rinsing with toluene and dried under nitrogen flow followed spin-coating of the polymer. Polymer films were spin-cast at 4000–5000 RPM in a glovebox from a 10 mg/mL solution in chloroform or chlorobenzene. (No significant solvent dependence on device performance was observed). Samples were dried at 60 °C for 30 min and then annealed at the desired temperature for 10 min in a glove box. FET mobility measurements were performed in a glovebox using a Keithley 4200 Semiconductor Parametric Analyzer and a Signotone Micromanipulator S-1160 probe station. Samples measured had channel lengths of 5 µm and channel widths of 1 mm.

Tapping Mode Atomic Force Microscopy (TMAFM): Samples consisting of n-type Si substrates with thermally grown 200 nm silicon dioxide, were cut, subject to the cleaning, UV-treatment, DTS-treatment, spin-casting and annealing treatment mentioned above. TMAFM studies were carried out in room-temperature air with an MFP-3D-SA Atomic Force Microscope made by Asylum Research. The probes were FORTA probes from Applied Nanostructures, which have a silicon cantilever of nominal spring constant of 3.0 N/m, a nominal resonance frequency of ~60 kHz, and were tuned to a RMS cantilever oscillation amplitude of ~1000 mV. Acquired images of 1µm x 500nm were taken with a scan frequency of 1 Hz.

X-ray diffraction measurements: Samples consisting of n-type Si substrates with thermally grown 200 nm silicon dioxide, were cleaned in acetone and isopropanol, dried in an oven at 120 °C for 15 min, and then exposed for 1.5 hrs to UV light in air. The devices were surface treated with DTS for 30 min by immersion in a 1% by volume of DTS in toluene. The devices were then cleaned by rinsing with toluene and dried under nitrogen flow. Polymer films were spin-cast on the passivated substrates at 5000 RPM in a glovebox from a 10mg/mL solution of chlorobenzene. Samples were dried at 60 °C for 30 min. The polymer films were then annealed at the optimized temperature for 10 min in a glove box. Specular XRD and grazing incidence XRD were performed on a Rigaku SmartLab diffraction system with a Cu Kα source, with specular measuring out-of-plane alignment and grazing incidence measuring both in-plane and out-of-plane alignments. For grazing incidence XRD, the incident beam was fixed at 0.2 degrees to stay below the critical angle of SiO_2. Samples were approximately 10 mm × 10 mm in size, and were measured with an integration time of 4min/degree for specular XRD and 10min/degree for grazing incidence XRD.

Synthesis of Monomer and Polymer, DSC data, Cyclic voltammetry data and UV/vis-NIR absorption spectrum: see Supporting Information.

Supporting Information

Supporting Information is available from the Wiley Online Library or from the author.

Acknowledgements

Support for J Fan through the Center for Energy Efficient Materials (CEEM) supported by the DOE as an EFRC. A portion of this work was done in the UCSB nanofabrication facility, part of the NSF funded NNIN network. Support for research was provided by the Air Force Office of Scientific Research (Charles Lee, Program Officer), the National Science Foundation Polymer program (Grant No. NSF-DMR-0856060).

Partial Support by DARPA through CBRITE corporation is gratefully acknowledged. J.D. Yuen thanks G. Hernandez-Sosa, S. Valouch, N. Banerji and J.H. Seo for useful discussions. J. Fan thanks W.B. Cui, T. Pho and Y. Lei for technical assistance and useful discussions.

Received: October 6, 2011
Revised: January 18, 2012
Published online: March 26, 2012

[1] a) H. Usta, A. Facchetti, T. J. Marks, *J. Am. Chem. Soc.* **2008**, *130*, 8580; b) M. Shkunov, R. Simms, M. Heeney, S. Tierney, I. McCulloch, *Adv. Mater.* **2005**, *17*, 2608; c) A. Babel, Y. Zhu, K. F. Cheng, W. C. Chen, S. A. Jenekhe, *Adv. Funct. Mater.* **2007**, *17*, 2542; d) E. J. Meijer, D. M. Deleeuw, S. Setayesh, E. Van Veenendaal, B.-H. Huisman, P. W. M. Blom, J. C. Hummelen, U. Scherf, T. M. Klapwijk, *Nat. Mater.* **2003**, *2*, 678; e) J. Cornil, J.-L. Brédas, J. Zaumseil, H. Sirringhaus, *Adv. Mater.* **2007**, *19*, 1791; f) K. Szendrei, D. Jarzab, Z. Chen, A. Facchetti, M. A. Loi, *J. Mater. Chem.* **2010**, *20*, 1317.

[2] a) L. Bürgi, M. Turbiez, R. Pfeiffer, F. Bienewald, H. J. Kirner, C. Winnewisser, *Adv. Mater.* **2008**, *20*, 2217; b) S. Cho, J. Lee, M. Tong, J. H. Seo, C. Yang, *Adv. Funct. Mater.* **2011**, *21*, 1910; c) P. Sonar, S. P. Singh, Y. Li, M. S. Soh, A. Dodabalapur, *Adv. Mater.* **2010**, *22*, 5409.

[3] Y. Li, S. P. Singh, P. Sonar, *Adv. Mater.* **2010**, *22*, 4862.

[4] a) J. C. Bijleveld, A. P. Zoombelt, S. G. J. Mathijssen, M. M. Wienk, M. Turbiez, D. M. de Leeuw, R. A. J. Janssen, *J. Am. Chem. Soc.* **2009**, *131*, 16616; b) J. C. Bijleveld, V. S. Gevaerts, D. Di Nuzzo, M. Turbiez, S. G. J. Mathijssen, D. M. de Leeuw, M. M. Wienk, R. A. J. Janssen, *Adv. Mater.* **2010**, *22*, E242.

[5] F. S. Kim, X. Guo, M. D. Watson, S. A. Jenekhe, *Adv. Mater.* **2010**, *22*, 478.

[6] a) T. Steckler, X. Zhang, J. Hwang, R. Honeyager, S. Ohira, X. Zhang, A. Grant, S. Ellinger, S. Odom, D. Sweat, D. Tanner, A. Rinzler, S. Barlow, J. Brédas, B. Kippelen, S. Marder, J. Reynolds, *J. Am. Chem. Soc.* **2009**, *131*, 2824; b) X. Zhang, T. T. Steckler, R. R. Dasari, S. Ohira, W. J. Potscavage, S. P. Tiwari, S. Coppee, S. Ellinger, S. Barlow, J. Brédas, B. Kippelen, J. R. Reynolds, S. R. Marder, *J. Mater. Chem.* **2010**, *20*, 123.

[7] K. Ono, S. Tanaka, Y. Yamashita, *Angew. Chem. Int. Ed. Engl.* **1994**, *33*, 1977.

[8] a) J. D. Yuen, R. Kumar, D. Zakhidov, J. Seifter, B. Lim, A. J. Heeger, F. Wudl, *Adv. Mater.* **2011**, *23*, 3780–3785; b) J. D. Yuen, J. Fan, J. Seifter, B. Lim, R. Hufschmid, A. J. Heeger, F. Wudl, *J. Am. Chem. Soc.* **2011**, *133*, 20799.

[9] a) Z. Chen, Y. Zheng, H. Yan, A. Facchetti, *J. Am. Chem. Soc.* **2009**, *131*, 8; b) H. Yan, Z. Chen, Y. Zheng, C. Newman, J. R. Quinn, F. Doetz, M. Kastler, A. Facchetti, *Nature* **2009**, *457*, 679.

[10] Z. Chen, H. Lemke, S. Albert-Seifried, M. Caironi, M. M. Nielsen, M. Heeney, W. Zhang, I. McCulloch, H. Sirringhaus, *Adv. Mater.* **2010**, *22*, 2371.

[11] J. D. Yuen, R. Kumar, J. Seifter, S. Valouch, D. Zakhidov, D. Moses, U. Lemmer, A. J. Heeger, F. Wudl, *J. Am. Chem. Soc.* **2011**, *133*, 19602–19605.

[12] a) E. J. Meijer, D. M. de Leeuw, S. Setayesh, E. van Veenendaal, B.-H. Huisman, P. W. M. Blom, J. C. Hummelen, U. Scherf, T. M. Klapwijk, *Nat. Mater.* **2003**, *2*, 678; b) J. Zaumseil, H. Sirringhaus, *Chemical Reviews* **2007**, *107*, 1296.

[13] a) T. D. Anthopoulos, D. M. de Leeuw, E. Cantatore, P. van't Hof, J. Alma, J. C. Hummelen, *J. Appl. Phys.* **2005**, *98*, 054503; b) T. D. Anthopoulos, D. M. de Leeuw, E. Cantatore, S. Setayesh, E. J. Meijer, C. Tanase, J. C. Hummelen, P. W. M. Blom, *Appl. Phys. Lett.* **2004**, *85*, 4205.